Geomagnetic EMP: Field Calculations

GÖSTA LJUNGDAHL

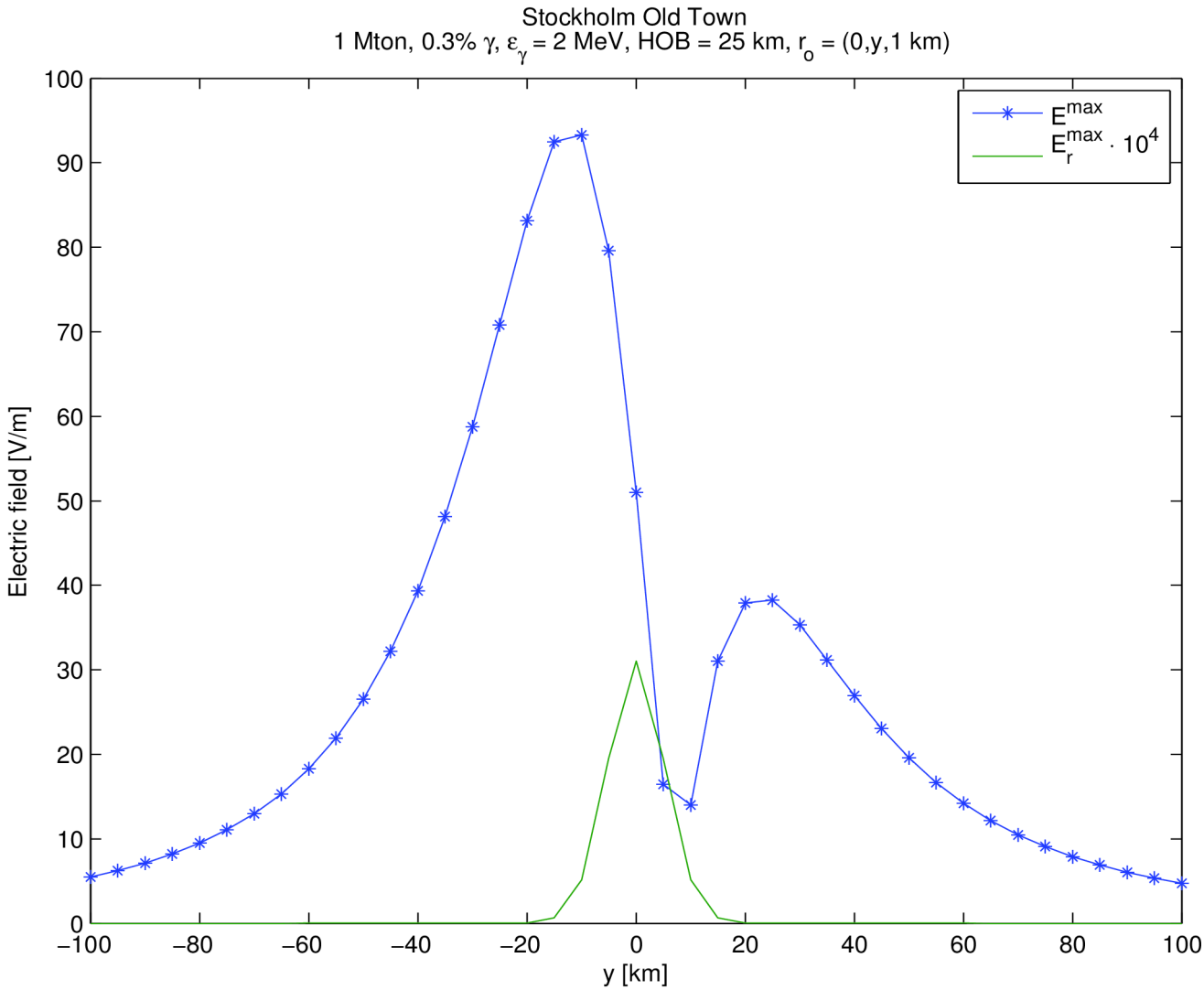

FOI-R--3795--SE
ISSN 1650-1942 December 2013

Gösta Ljungdahl

Geomagnetic EMP: Field Calculations

Cover picture
Blue: Maximum EMP electric field along the meridian through Stockholm Old Town as obtained by model calculations. The curve is consistent with "happy face" contour plots often found in EMP contexts. The indicated levels are small compared to independent results. Green: Maximum radial component of the electric field, up-scaled with a factor of 10^4.

Titel	Geomagnetisk EMP: Fältberäkningar
Title	Geomagnetic EMP: Field Calculations
Report no	FOI-R--3795--SE
Month	December
Year	2013
Pages	38
ISSN	ISSN-1650-1942
Customer	The Swedish MFA
Project no	A290211
Approved by	Nils Olsson Head, Defence and Security, Systems and Technology
Division	Defence & Security, Systems and Technology

FOI Swedish Defence Research Agency

Abstract

This report presents improvements on a theory describing the electromagnetic fields generated by prompt gamma radiation from a low altitude (up to 25 km) nuclear explosion, the so called electromagnetic pulse, EMP. It examines in some detail various parameters from the point of view of making a computer program implementation. The contribution to the EMP from the air-ground(sea surface) discontinuity is not taken into account.

Example calculations of current density, secondary electron conductivity and electric field are given for some illustrative cases. It is demonstrated that the main contribution to the EMP due to synchrotron radiation comes from a comparatively small region around the explosion thereby giving some credit to the use of constant approximations to non-constant parameters. Comparison is made with results from the original formulation showing that the theoretical improvements do not have a big numerical impact on the magnitude of the electric field except relatively close to the explosion. By comparison with openly published data it is shown that the C++ program used for calculation at its current state gives results that generally are considerably smaller except for altitudes 10 km and above and not very far away from the explosion.

Finally an outlook is given listing outstanding issues to be addressed in future work, e.g.(not in order of priority), investigation of parameters related to the current and conductivity calculation, reformulation of the C++ code describing the magnetic field dependence, self-consistent calculations of magnetic field and current density, investigation of absorption processes for the secondary electrons and influence of, e.g., different types of weapon.

Keywords

EMP, GEMP, SREMP, Compton scattering, synchrotron radiation, primary electrons, secondary electrons

Sammanfattning

Föreliggande rapport presenterar en förbättrad formulering av en teori som beskriver den elektromagnetiska puls, EMP, som skapas av direkt gammastrålning från en kärnexplosion på låg höjd (upp till 25 km) i atmosfären. I teorin kartläggs också begränsningar av diverse parametrar och hur dessa påverkar implementeringen av ett datorprogram. Bidraget till EMP från den diskontinuitet som övergången mellan luft och mark (eller hav) ger upphov till behandlas inte.

Beräkningar av strömtäthet, konduktivitet och elektriskt fält ges för några illustrativa fall. Beräkningarna visar att bidraget till EMP huvudsakligen kommer ifrån ett förhållandevis litet område kring explosionen vilket i någon mån kan försvara användningen av konstanta approximationer till icke-konstanta parametrar. En jämförelse görs med resultat beräknade med orignalformuleringen av vilken det framgår att de teoretiska förbättringarna inte har ett stort inflytande på beräkning av det elektriska fältet utom relativt nära explosionen. Öppet publicerade data redovisar resultat som i allmänhet är betydligt större utom för höjder större än 10 km och inte alltför långt från explosionen.

Slutligen listas tänkbara områden för fortsatt arbete som t.ex.: undersökning av parametrar relaterade till beräkning av ström och konduktivitet, omkodning av magnetfältsberoendet, implementering av självkonsistenta beräkningar av magnetfält och strömtätheter, undersökning av absorptionsprocesser för sekundärelektroner samt undersökning av vilken påverkan t.ex. vapentypen har.

Nyckelord

EMP, GEMP, SREMP, Comptonspridning, synkrotronstrålning, primärelektroner, sekundärelektroner

Contents

1 Introduction

A nuclear explosion generates a rapidly growing electromagnetic pulse, EMP, which is a potential hazard to all electronic equipment. It is therefore of interest to estimate the magnitude of the electric and magnetic fields generated and the area over which the EMP has a potentially dangerous strength. Most of the development in this respect was done in the late 1950s and early 1960s [1, 2, 3]. The area of study has since resulted in occasional papers, e.g., ref. [4, 5]. A recent article by Roussel-Dupré [6], appearing in 2005, gives further support to the main ideas developed half a century earlier by showing identical results using two different approaches.

The basic mechanisms generating prompt EMP are as follows: The nuclear explosion generates a more or less spherically symmetric flow of X-rays, γ-rays and neutrons of which the γ-rays and X-rays travel outwards at the speed of light. The high energy γ-photons undergo Compton scattering against the electrons of the molecules in the atmosphere. The binding energy of the electrons in the molecules is small compared to the energy of the γ-photons and the electrons are therefore effectively free. During the scattering process the electrons gain momentum primarily in the forward direction. These so called primary electrons, or Compton electrons, give rise to a current, the Compton current, flowing outwards from the point of the nuclear explosion. Transverse electromagnetic fields are generated if the Compton current acquires asymmetry, otherwise the electric fields of the EMP would be small. Asymmetry can be caused by, e.g.,

- Differential absorption of γ-photons, e.g., atmosphere-earth interface
- Weapon design
- Air density gradient
- Interaction with the geomagnetic field.

Secondary electrons are generated by primary electrons as they hit and ionize the atmosphere molecules. The secondary electrons and ions are slow compared to the primary electrons. The conductivity so produced effectively constitutes an electric resistance to the Compton current and so causes a drop in the magnitude of the EMP. Both ions and electrons contribute to the conductivity but the electrons dominate by virtue of their smaller mass. At low altitudes X-rays are absorbed in the atmosphere within a few meters and do not contribute to the EMP. At higher altitudes they contribute to the secondary electrons by the photoelectric effect. Neutrons scatter in-elastically and get captured by the air molecules and produce secondary γ-photons that in turn generate Compton electrons. The EMP is, however, at early times determined by the prompt Compton electrons together with the generated conductivity. The geomagnetic field gives rise to synchrotron radiation from the Compton electrons and it is this particular asymmetry, the last in the list above, that the article by Roussel-Dupré discusses. The corresponding EMP is called Geomagnetic EMP or GEMP. Another name often encountered in the literature is SREMP (Source Region EMP). Geomagnetic interaction is also the basic mechanism in HEMP (high altitude EMP). The derivation of the synchrotron radiation field in ref. [6] assumes nuclear bursts below 25 km as the treatment of the secondary electrons ignores their momentum transfer and assumes that collisions

are frequent enough that the secondary electrons reach equilibrium with the electric field. It also considers only the prompt γ-pulse, i.e. is limited to times earlier than 2 μs from the nuclear blast.

The present report reviews parts of the theory in ref. [6] which is the theoretical basis of an ongoing effort to implement a computer program for calculation of the EMP electric field and provides an expression for the radial electric field which Roussel-Dupré has chosen to omit. In addition the report improves the treatment of the primary electron loss and compares the results using the original treatment and the improved for some illustrative cases. The report is organised in the following fashion. An alternative solution of the differential equation governing the motion of the primarily electrons is presented and it is shown that this solution is more satisfactory in terms of primary electron loss. Then follows a discussion of the γ-photon mean free path and its dependence on altitude after which the γ-flux is described. The relevant formulation of Maxwell's equations for the electric field is presented together with solutions thereof. As the electric field solutions require knowledge of the conductivity a derivation of this quantity starting from the time rate of change of the primary and secondary electron densities is presented. The review of the theory concludes with models or values for various parameters required for the computation of the electric fields. The last part of the report is devoted to example calculations first of currents and conductivities and then of fields giving some insight into the behaviour of the model, e.g., it is demonstrated that the improved treatment of the primary electron loss in most cases does not have a dramatic numerical influence. The report ends with a discussion of observations made and suggestion of what to do next.

2 Theory

The theory presented here is a development of the one presented by Roussel-Dupré [6] in the first part of his article. Essentially the electric fields are calculated using Maxwell's equations where the current density is derived using a plasma physics approach. The calculation of the current density involves coupled differential equations for the number density and the momentum density of the primary and secondary electrons. At low altitudes the atmosphere is thick enough that the momentum density equation for the secondary electrons may be dropped [7]. Roussel-Dupré then transforms the equations into a frame moving at the speed of light along the γ-rays, i.e. a Lorentz transformation and introduces the retarded time defined by $\tau = (t - r/c_0)$, where r is the distance between the observer and the field point and c_0 the speed of light. Roussel-Dupré employs a number of approximations and assumptions, among other things the so called high frequency approximation which essentially says that time derivatives are much larger (in an absolute sense) than divergences ($\bigtriangledown\cdot$), leading to equation (2.1) below in CGS-Gaussian units. For details regarding the procedure the reader is referred to the article by Roussel-Dupré [6]. See also comments below in section 2.2.1.

2.1 Current Density

The starting point is equation (9) in Roussel-Dupré's article, essentially an equation of motion for the primary electrons, which reads

$$(1 - \beta_{pr})\frac{\partial \boldsymbol{j}_p}{\partial \tau} = -\nu \boldsymbol{j}_p - F_\gamma e v_0 \hat{\boldsymbol{r}}/\lambda_c - \Omega \boldsymbol{j}_p \times \hat{\boldsymbol{B}}. \tag{2.1}$$

Here β_{pr} is a result of the Lorentz transformation and denotes the ratio of the primary electron speed to the speed of light, $\boldsymbol{j}_p$ the primary current density, τ the retarded time, ν the momentum loss rate, F_γ the γ-ray flux (see section 2.1.2 below), e the electron charge, v_0 the primary electron speed (assumed to be constant), $\hat{\boldsymbol{r}}$ the distance unit vector, λ_C the Compton attenuation length or the mean free path of the γ-quanta, Ω the electron Larmor angular frequency and $\hat{\boldsymbol{B}}$ a unit vector in the direction of the magnetic field. The geometry is shown in figure 2.1 which also defines the polar coordinate system together with the associated Cartesian system.[1] With a change of notation the equation can be written as

$$\frac{\partial \boldsymbol{j}_p}{\partial \tau} = -\nu' \boldsymbol{j}_p - F(\tau)\hat{\boldsymbol{r}} - \Omega' \boldsymbol{j}_p \times \hat{\boldsymbol{B}}. \tag{2.2}$$

Roussel-Dupré drops the loss term $-\nu' \boldsymbol{j}_p$ leaning on Karzas and Latter [3] and then solves the equation. The loss of primary electrons is then taken into account by setting the inverse of ν' as the upper limit of the resulting integration in the solution. The corresponding physical model is that all primary electrons have the same life time after which they all vanish simultaneously. This is not a very realistic model but may have negligible numerical influence in certain cases.

It is not entirely clear why Roussel-Dupré has chosen to solve the current density equation in this fashion as it is not likely that the possibility of keeping

[1] The reader may wonder why the zero of the ϕ-coordinate is not indicated. The reason is that the zero is arbitrary as neither the ϕ unit vector nor the theory depends on the actual value of ϕ. It is for the same reason not necessary to specify $\hat{\mathrm{x}}$ and $\hat{\mathrm{y}}$.

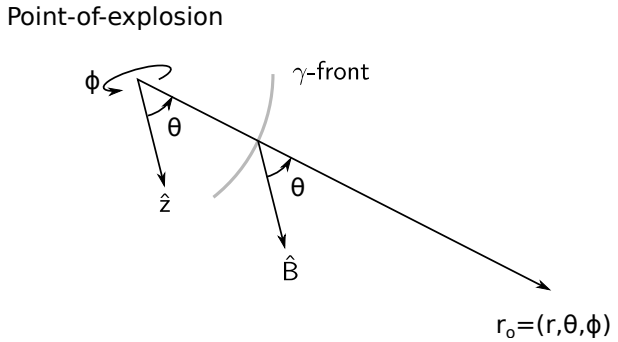

Figure 2.1: Schematic diagram showing point-of-explosion and point-of-observation. The direction of the magnetic field is indicated by $\hat{\mathbf{B}}$. The polar coordinate system is defined where $\hat{\mathbf{z}}$ denotes the z-direction (parallel to the magnetic field) of the associated Cartesian coordinate system. The position of the γ-front at some time before it reaches the point of observation is indicated by the grey arc.

the loss term has been overlooked. The reason could be that if the loss term is kept then complete agreement is not obtained with the result Roussel-Dupré presents in the second part of his article in which he derives the electric fields using the Leonard-Wiechert potentials [8].

It is, as has been hinted above, not necessary to drop the loss term in order to solve the equation. The Cartesian component equations at a field point specified by (r, θ, ϕ) relative to the point of explosion ($\hat{z}$ is defined parallel to the magnetic field) are

$$\begin{aligned} \frac{\partial j_{px}}{\partial \tau} &= -\nu' j_{px} - \Omega' j_{py} - F(\tau)\sin\theta\cos\phi \\ \frac{\partial j_{py}}{\partial \tau} &= \Omega' j_{px} - \nu' j_{py} - F(\tau)\sin\theta\sin\phi \\ \frac{\partial j_{pz}}{\partial \tau} &= -\nu' j_{pz} - F(\tau)\cos\theta. \end{aligned} \tag{2.3}$$

The process of solving (2.3) can be started by noting that the third equation is not coupled to the other two and so can be solved with the aid of an integrating factor, $e^{\nu'\tau}$. We find that

$$j_{pz}(\tau) = -e^{-\nu'\tau}\int_0^\tau F(\tau')e^{\nu'\tau'}\cos\theta d\tau' = -\int_0^\tau F(\tau')e^{-\nu'(\tau-\tau')}\cos\theta d\tau'. \tag{2.4}$$

The first two equations are rewritten using matrix notation giving

$$\frac{\partial \boldsymbol{j}_{pt}}{\partial \tau} = \frac{\partial}{\partial \tau}\begin{pmatrix} j_{px} \\ j_{py} \end{pmatrix} = \begin{pmatrix} -\nu' & -\Omega' \\ \Omega' & -\nu' \end{pmatrix}\boldsymbol{j}_{pt} + \boldsymbol{F}(\tau), \tag{2.5}$$

where $\boldsymbol{j}_{pt} = \boldsymbol{j}_p - j_{pz}\hat{z}$ and

$$\boldsymbol{F}(\tau) = \begin{pmatrix} -F(\tau)\sin\theta\cos\phi \\ -F(\tau)\sin\theta\sin\phi \end{pmatrix}. \tag{2.6}$$

The eigenvalues of the coefficient matrix are $\lambda_\pm = -\nu' \pm i\Omega'$ and corresponding eigenvectors are, for instance,

$$\boldsymbol{v}_+ = \begin{pmatrix} e^{i\frac{\pi}{2}} \\ 1 \end{pmatrix} \text{ and } \boldsymbol{v}_- = \begin{pmatrix} 1 \\ e^{i\frac{\pi}{2}} \end{pmatrix}.$$

The general solution to the homogeneous part of (2.5) is then given by

$$\boldsymbol{j}_{pt,h} = e^{-\nu'\tau} \begin{pmatrix} e^{i(\frac{\pi}{2}+\Omega'\tau)} & e^{-i\Omega'\tau} \\ e^{i\Omega'\tau} & e^{i(\frac{\pi}{2}-\Omega'\tau)} \end{pmatrix} \boldsymbol{c} \equiv B(\tau)\boldsymbol{c}, \tag{2.7}$$

where $\boldsymbol{c}$ is an arbitrary constant vector. Note that $B(\tau)$ defined above is not to be confused with the magnetic field.

By allowing $\boldsymbol{c}$ to vary a particular solution can be constructed which vanishes for $\tau = 0$. Differentiating the homogeneous solution (2.7) with $\boldsymbol{c}{=}\boldsymbol{c}(\tau)$ gives

$$\frac{\partial \boldsymbol{j}_{pt,h}}{\partial \tau} = \frac{\partial B(\tau)}{\partial \tau}\boldsymbol{c} + B(\tau)\frac{\partial \boldsymbol{c}}{\partial \tau}. \tag{2.8}$$

Identification of terms by comparing with eq. (2.5) yields

$$B(\tau)\frac{\partial \boldsymbol{c}}{\partial \tau} = \boldsymbol{F}(\tau) \tag{2.9}$$

from which

$$\boldsymbol{c}(\tau) = \int_0^\tau B^{-1}(\tau')\boldsymbol{F}(\tau')d\tau' \tag{2.10}$$

provided that $B(\tau)$ is invertible and that $\boldsymbol{c}(\tau = 0) = 0$ of which the latter obviously is satisfied. The inverse exists as the determinant $|B(\tau)| = -2e^{-\nu'\tau} \neq 0$ and is

$$B^{-1}(\tau') = \frac{e^{\nu'\tau'}}{2} \begin{pmatrix} -e^{i(\frac{\pi}{2}-\Omega'\tau')} & e^{-i\Omega'\tau'} \\ e^{i\Omega'\tau'} & -e^{i(\frac{\pi}{2}+\Omega'\tau')} \end{pmatrix}. \tag{2.11}$$

The particular solution can now be expressed as

$$\boldsymbol{j}_{pt,p} = B(\tau)\boldsymbol{c}(\tau) = B(\tau)\int_0^\tau B^{-1}(\tau')\boldsymbol{F}(\tau')d\tau' \equiv \int_0^\tau G(\tau-\tau')\boldsymbol{F}(\tau')d\tau', \tag{2.12}$$

where the Green's matrix,

$$G(\tau-\tau') = e^{-\nu'(\tau-\tau')} \begin{pmatrix} \cos\Omega'(\tau-\tau') & -\sin\Omega'(\tau-\tau') \\ \sin\Omega'(\tau-\tau') & \cos\Omega'(\tau-\tau') \end{pmatrix}, \tag{2.13}$$

is defined.

Equations (2.6), (2.12) and (2.13) now give the components of the particular solution as

$$\begin{aligned} j_{px}(\tau) &= -\int_0^\tau F(\tau')e^{-\nu'(\tau-\tau')} \\ &\quad \cdot [\sin\theta\cos\phi\cos\Omega'(\tau-\tau') - \sin\theta\sin\phi\sin\Omega'(\tau-\tau')]\, d\tau' \\ j_{py}(\tau) &= -\int_0^\tau F(\tau')e^{-\nu'(\tau-\tau')} \\ &\quad \cdot [\sin\theta\cos\phi\sin\Omega(\tau-\tau') + \sin\theta\sin\phi\cos\Omega(\tau-\tau')]\, d\tau'. \end{aligned} \tag{2.14}$$

A change of variables, $\tau - \tau' = \tau''$, then yields

$$\begin{aligned} j_{px}(\tau) &= \int_\tau^0 F(\tau-\tau'')e^{-\nu'\tau''} \\ &\quad \cdot [\sin\theta\cos\phi\cos\Omega'\tau'' - \sin\theta\sin\phi\sin\Omega'\tau'']\, d\tau'' \\ j_{py}(\tau) &= \int_\tau^0 F(\tau-\tau'')e^{-\nu'\tau''} \\ &\quad \cdot [\sin\theta\cos\phi\sin\Omega'\tau'' + \sin\theta\sin\phi\cos\Omega'\tau'']\, d\tau'' \\ j_{pz}(\tau) &= \int_\tau^0 F(\tau-\tau'')e^{-\nu'\tau''}\cos\theta d\tau''. \end{aligned} \tag{2.15}$$

Compared to Roussel-Dupré's result the solution now includes the loss of Compton electrons at the same level of approximation as the differential equation (2.1). Moreover, the form of the current build-up is intuitively correct. An early contribution, where the argument of $F(\cdot)$ is near zero, suffers a large loss because τ'' is near its maximum value whereas a late contribution (τ'' near zero) suffers a small loss. Dropping the notation shorthand introduced in (2.2) and converting to polar coordinates yields

$$\begin{aligned} j_r(r,\tau) &= \tfrac{ev_0}{\lambda_c}\int_\tau^0 \tfrac{F_\gamma(r,\tau-\tau'')}{1-\beta_r} e^{-\frac{\nu\tau''}{1-\beta_r}}(\cos^2\theta+\sin^2\theta\cos\Omega'\tau'')d\tau'' \\ j_\theta(r,\tau) &= \tfrac{ev_0}{\lambda_c}\int_\tau^0 \tfrac{F_\gamma(r,\tau-\tau'')}{1-\beta_r} e^{-\frac{\nu\tau''}{1-\beta_r}}\cos\theta\sin\theta(\cos\Omega'\tau''-1)d\tau'' \\ j_\phi(r,\tau) &= \tfrac{ev_0}{\lambda_c}\int_\tau^0 \tfrac{F_\gamma(r,\tau-\tau'')}{1-\beta_r} e^{-\frac{\nu\tau''}{1-\beta_r}}\sin\theta\sin\Omega'\tau''d\tau''. \end{aligned} \tag{2.16}$$

The expressions (2.16) correspond to Roussel-Dupré's solution [6, eq. (10)-(12)]. Note that the change of integration variable causes the integration to go backwards mathematically although still forward in time. Roussel-Dupré introduces a minus-sign to make the integration go forward mathematically but then it goes backwards in time working its way back towards the time of explosion. The change of integration variables serves no clarification purpose but has been retained partly to arrive at an analogous form and partly for historical reasons related to the computer program used for calculations. Note also the absence of ϕ in (2.16) and that if θ equals zero, i.e. the Compton current is parallel to the magnetic field then there is only radial current which means that there will be no transverse electric fields, i.e. minimum EMP, see eq. (2.25) further down.

2.1.1 The Gamma-photon Mean Free Path

Mean free paths for particles in the atmosphere are generally inversely proportional to the density which depends on the altitude. This is also the case for λ_C appearing in the equations above, i.e.

$$\lambda_C(\rho(z)) = \lambda_C(\text{sea level})\frac{\rho(\text{sea level})}{\rho(z)}, \tag{2.17}$$

where $\lambda_C(\text{sea level}) = 300$ m [3]. For a field point below the explosion and at a distance r from it we can express the density according to $\rho(z) = \rho(z_e - r\cos(\vartheta))$ where z_e is the explosion altitude and ϑ is the angle between the vertical and the line-of-sight. The density can be obtained from the U.S. Standard Atmosphere 1976 [9] as a function of altitude. The standard atmosphere consists of seven layers up to an altitude of 86 km and is for the parts used here the same as the international standard atmosphere, ISA [10]. The dependence on altitude is near exponential and it is quite common in the EMP literature to assume that λ_C increases exponentially with altitude. Roussel-Dupré has provided such a model for λ_C [7]

$$\lambda_C(r_f) = \lambda_C(\text{sea level})e^{\frac{z_e - r\cos(\vartheta)}{700000}} \tag{2.18}$$

where all lengths are measured in cm. 700000 cm = 7 km is the "average scale height" of the atmosphere, i.e. the altitude at which the pressure has dropped to $1/e$ of the sea level value.

2.1.2 The Gamma-ray Flux

The integral over a closed surface (e.g., a sphere) surrounding the nuclear burst for all times from the time of the burst of the γ-ray flux, $F_\gamma(r,\tau)$, results in

the total γ-yield of the explosion minus whatever amount has been lost due to attenuation. This suggests that a suitable form is the total yield per unit area compensated for the attenuation of the γ-photons at the surface of the sphere multiplied by a distribution function starting at $\tau = 0$ and that integrates to unity over all times. The distribution function should be such as to mimic the rise and fall of γ-photons over time. The realisation employed here, one of several listed in ref. [11], is

$$f(t) = \frac{e^{-c_1\tau} - e^{-c_2\tau}}{c_1^{-1} - c_2^{-1}},$$

where the constants $c_1 = 2 \cdot 10^8$ s^{-1} and $c_2 = 3 \cdot 10^8$ s^{-1}, see figure 2.2.

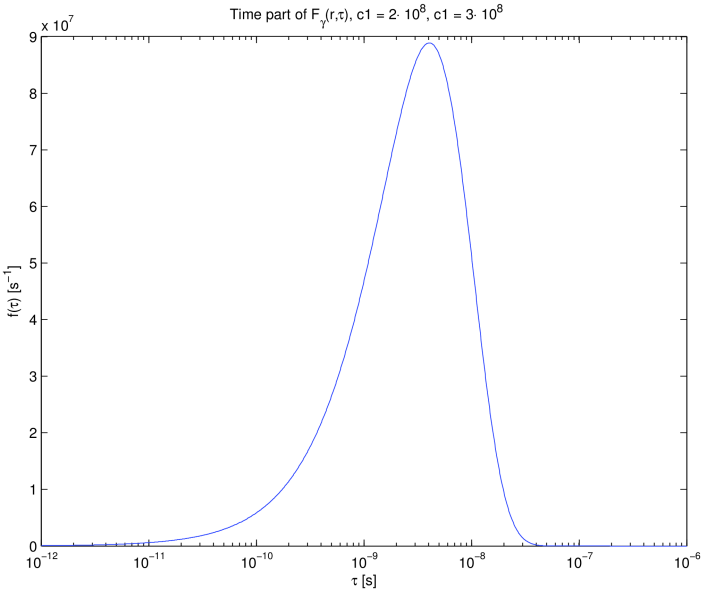

Figure 2.2: Time distribution function for the γ-pulse.

It remains to estimate the γ-yield. The yield of a bomb is customarily measured in terms of equivalent tons TNT where 1 kton = 4.184 TJ. The gamma energy spans over a wide range of energies from a few hundred keV to several MeV but it suffices here to use a mean energy ε_γ. It is also assumed that all γ-photons undergo Compton scattering, i.e. the number of generated primary electrons equals the number of γ's. Only a small amount of the total energy corresponds to γ radiation. Exactly how much depends on the nuclear device but varies between 0.1-0.5 % [12, 13]. The γ-yield is:

$$Y_\gamma = Y \cdot 4.184 \cdot 10^{12} \cdot \frac{\eta_\gamma}{\varepsilon_\gamma},$$

where Y is the bomb yield in kilotons, η_γ is the γ efficiency and ε_γ has to be given in Joules, leading to

$$F_\gamma(r,\tau) = \frac{Y_\gamma e^{-r/\lambda_C}(e^{-c_1\tau} - e^{-c_2\tau})}{4\pi r^2(c_1^{-1} - c_2^{-1})}, \tag{2.19}$$

which is valid if λ_C is constant for all r along the line-of-sight. This, however, is generally not the case as λ_C depends on the air density which is constant

only for field points at the same altitude as the explosion. The dependence on altitude translates for a particular line-of-sight to a dependence on r since z_e and ϑ, introduced in the previous section, are constant. To accommodate this dependence the expression has to be modified according to

$$F_\gamma(r,\tau) = \frac{Y_\gamma e^{-\int_0^r \frac{dr'}{\lambda_C(r')}}(e^{-c_1\tau} - e^{-c_2\tau})}{4\pi r^2(c_1^{-1} - c_2^{-1})}. \tag{2.20}$$

Both forms of the attenuation factor in the equations above are encountered in the literature, cf. ref. [2, 4, 6, 11] and in some cases it doesn't matter much which one is used as will be shown further down in section 3.2.

It should be mentioned that the solution for the current density presented above, i.e. eq. (2.16), eliminates a causality problem present in Roussel-Dupré's formulae [6, eq. (10)-(12)] in which it is possible for the time argument of the gamma ray flux to become negative. A negative time argument in F_γ would mean a time before the burst and of course no γ. This problem had passed unnoticed at the time of writing of [6]. A rather obvious remedy is to require $F_\gamma(r,\tau) = 0$ for $\tau < 0$.

2.2 Electric Field

In the high frequency approximation the polar components of the relevant Maxwell equations take the form [3, 11]

$$\frac{\partial E_r}{\partial \tau} = -4\pi(j_r + \sigma E_r) \tag{2.21}$$

$$\frac{1}{r}\frac{\partial r E_\theta}{\partial r} = -\frac{2\pi}{c_0}(j_\theta + \sigma E_\theta) \tag{2.22}$$

$$\frac{1}{r}\frac{\partial r E_\phi}{\partial r} = -\frac{2\pi}{c_0}(j_\phi + \sigma E_\phi), \tag{2.23}$$

where σ is the conductivity.

Equation (2.21) can be integrated using the integrating factor $e^{4\pi\int\sigma(\tau)d\tau}$ leading to

$$E_r(r,\tau) = -4\pi\int_0^\tau j_r(r,\tau'')e^{-4\pi\int_{\tau''}^{\tau}\sigma(r,\tau')d\tau'}d\tau''. \tag{2.24}$$

Equations (2.22) and (2.23) have the same form and can be integrated if one considers instead the variable $\varepsilon_{\theta,\phi} = rE_{\theta,\phi}$. The solutions are then readily found using the integrating factor $e^{\frac{2\pi}{c_0}\int\sigma(r)dr}$ which, after division by r, results in

$$E_{\theta,\phi}(r,\tau) = -\frac{2\pi}{rc_0}\int_0^r r' j_{\theta,\phi}(r',\tau)e^{-\frac{2\pi}{c_0}\int_{r'}^{r}\sigma(r'',\tau)dr''}dr'. \tag{2.25}$$

The presence of the secondary electrons constitutes a resistance, as has been mentioned above in chapter 1, which is manifest in the integration factors via its inverse, the conductivity. As the conductivity is positive the argument of the exponential functions is always negative. Hence the integration factors have an upper limit of one. Therefore an upper limit of the electric field magnitude may be obtained by dropping the integration factors from the integrals. A lower bound requires a closer examination of the conductivity and the integration limits to find the smallest possible value of the exponent.

2.2.1 Secondary Electron Density

The field integrals, eq. (2.24, 2.25), contain the conductivity in the exponent of the integrating factor. The main contribution to the conductivity is the secondary electrons. Equations (1) and (3) in ref. [6] describe the densities of primary and secondary electrons and read

$$\frac{\partial n_p}{\partial t} = - \bigtriangledown \cdot (n_p \mathbf{v}_p) + F_\gamma/\lambda_C - \nu_E n_p \tag{2.26}$$

$$\frac{\partial n_s}{\partial t} = - \bigtriangledown \cdot (n_s \mathbf{v}_s) - \alpha n_s + \nu_i n_s + \left(\frac{\varepsilon_p}{34}\right) \nu_E n_p. \tag{2.27}$$

The equations above describe the time rate of change of particle density, $n_{p,s}$, in unit volumes moving along the flows of primary and secondary electrons. Here $\mathbf{v}_{p,s}$ denotes the speed of the electrons, ν_E is the normalised energy loss rate for primary electrons, α is the electron capture coefficient for secondary electrons (several processes are possible, see [6, 4]), ν_i is the ionisation rate for secondary electrons and ε_p finally is the energy in eV of the primary electrons which in this model is constant.The factor 34 in the last term in eq. (2.27) arises because 34 eV is the energy consumed when a primary electron ionises an air molecule. λ_C (the γ attenuation length) is approximately 300 m at sea level and increasing upwards, i.e. very long compared to the width of the γ-front, which typically is a few meters. Transformation to a frame moving at the speed of light with the γ-front, retarded time and the above mentioned high frequency approximation thus allows neglect of the divergences of the particle streams, $n_{p,s}\mathbf{v}_{p,s}$. The time derivative will therefore dominate over the divergence of the primary electron streams and the same goes for the secondary electrons as their main contribution is ionisation of air molecules when hit by primary electrons. The speed of the secondary electrons is also assumed to be very small compared to that of the primary electrons which means that their momentum can be ignored. This assumption does not hold at high altitudes where the atmosphere is much thinner. For lower altitudes it is, however, sufficient to consider only the number density of the secondary electrons. Thus the high frequency approximations of eq. (2.26) and (2.27) are

$$(1 - \beta_r)\frac{\partial n_p}{\partial \tau} = F_\gamma/\lambda_C - \nu_E n_p$$

and

$$\frac{\partial n_s}{\partial \tau} = -\alpha n_s + \nu_i n_s + \left(\frac{\varepsilon_p}{34}\right) \nu_E n_p,$$

respectively. In principle the equation for the secondary electron density should be adjusted with a factor like $(1 - \beta_r)$ but since the speed of the secondary electrons is very small compared to c_0 the adjustment is negligible.[2] Collecting terms allows us to write

$$\frac{\partial n_p}{\partial \tau} + \frac{\nu_E}{(1 - \beta_r)} n_p = \frac{F_\gamma}{\lambda_C(1 - \beta_r)}$$

$$\frac{\partial n_s}{\partial \tau} - (\nu_i - \alpha) n_s = \left(\frac{\varepsilon_p}{34}\right) \nu_E n_p$$

Integrating factor for the primary electron density is $e^{\nu_e \tau/(1-\beta_r)}$ and for the secondary electron density $e^{-(\nu_i - \alpha)\tau}$ leading to the solutions

$$n_p(r, \tau) = \frac{1}{\lambda_C(1 - \beta_r)} \int_0^\tau F_\gamma(r, \tau') e^{-\nu_E(\tau - \tau')/(1-\beta_r)} d\tau' \tag{2.28}$$

[2]Note that because the primary electron energy is divided by the energy it takes to create a secondary electron it is OK to use any unit of energy as the ratio is dimensionless.

and

$$n_s(r,\tau) = \left(\frac{\varepsilon_p}{34}\right)\nu_E \int_0^\tau e^{(\nu_i-\alpha)(\tau-\tau')} n_p(r,\tau')d\tau', \tag{2.29}$$

corresponding to equation (13) in [6]. Note that quantities not explicitly dependent on τ are local, i.e. determined by the position.

2.2.2 Conductivity

Both ions and secondary electrons contribute to the conductivity. The ions, however, have much larger inertia and so their contribution can be ignored giving

$$\sigma(r,\tau) = \mu_e n_s(r,\tau)e = \mu_e(\text{sea level})\frac{\rho(\text{sea level})}{\rho} n_s(r,\tau)e, \tag{2.30}$$

where the electron mobility, μ_e, has a sea level value of 0.3 $\text{m}^2/\text{V}\cdot\text{s}$ (SI)[3] and is assumed to be inversely proportional to the density [4, eq. (17-18)]. The mobility is defined as the ratio of speed to electric field and the sea level value quoted assumes an electric field of about 10 kV/m [14].

2.2.3 Computational Engine

Equations (2.24), (2.25) and (2.16) form the theoretical solution for the electric field together with the equations (2.30) and (2.20) for the conductivity and the source of γ-photons. Models for λ_C have been presented in section 2.1.1. To form a complete computational framework numerical values for remaining parameters [15, eq. (12)-(15)] must also be defined. So far we have the relativistic mean speed of the primary electrons [16]

$$v_0 = c_0\sqrt{1 - \frac{m_e^2 c_0^4}{e^2\varepsilon_p^2}}, \tag{2.31}$$

where ε_p is given in eV and m_e denotes the electron mass.[4] The Larmor angular frequency adjusted as a consequence of the notation shorthand introduced in eq. (2.2)

$$\Omega' = \frac{\Omega}{1-\beta_r} = \frac{eB}{\gamma_p m_e c_0(1-\beta_r)}, \tag{2.32}$$

where $\gamma_p = (1-\beta_r^2)^{-1/2}$ is the Lorentz factor and B the magnitude of the geomagnetic field. If scattering of the primary electrons is neglected we may replace ν by ν_E which is estimated as the inverse of the primary electron lifetime. This is given by the primary electron mean free path or stopping range divided by the speed. The stopping range is a few meters at sea level, cf. ref. [3, 12, 14], and is assumed to be inversely proportional to the density. We have in CGS-Gaussian units

$$\nu_E = \frac{v_0\rho}{300\rho(\text{sea level})}. \tag{2.33}$$

One might be led to believe that since ν_E is proportional to the density, i.e. dependent on position, a modification similar to that of the γ attenuation factor

[3] 0.3 $\text{m}^2/\text{V}\cdot\text{s}$ (SI) = $\frac{3000}{1/300}$ $\text{cm}^2/\text{statV}\cdot\text{s} = 9\cdot 10^5$ $\text{cm}^2/\text{statV}\cdot\text{s}$ (CGS-Gauss)

[4] The total energy, $E_{tot} = E_k + m_e c_0^2$, that goes into the denominator under the root of eq. (2.31) has been approximated by the kinetic energy. It is a simple exercise to show that the mass energy equivalent is negligible in comparison. Also note that any system of units can be used under the square root.

is necessary. However, in all equations above ν_E is strictly a local parameter and its dependence on position is accounted for by means of eq. (2.33).

Remaining parameters to be set or modelled are ν_i and α of which the latter according to Longmire [4] has a typical sea level value of $1 \cdot 10^8$ s^{-1} and scales with the square of the density. The ionisation rate ν_i should have a dependence like ν_E, i.e. proportional to the density.

3 Example Calculations

The ultimate aim is to implement a model ready to use for reliable computation of expected electric field levels due to the EMP. This report covers several steps along the way but there is still some way to go. More on this further down in chapter 4. The calculations of various quantities shown here serve the purpose of acquiring knowledge about how the model behaves and to shed some light over the relative importance of various parameters and to give a rough idea of what to expect in terms of field levels. In all the calculations related to this model ν_i has been set to 0.1 s^{-1} apart from parameter values already mentioned. So far the author has not carried out any major attempt to investigate used parameter values. The point-of-explosion is specified by latitude, longitude and altitude. The point-of-observation is specified by a Cartesian coordinate system (not associated with the polar coordinate system mentioned earlier) with $\hat{x}$ pointing east, $\hat{y}$ pointing north and $\hat{z}$ pointing upwards. The origin of this coordinate system is at ground zero, i.e. the point on the surface of the earth directly below the explosion. Before presenting the calculations a note about units is in order.

3.1 Units

It is quite common in American literature related to EMP to use different systems of units depending on the context. Commonly volt and ampere have the same meaning as in SI. Indeed, the unit eV is commonly used in the sense it derives from SI for the energy of a γ-particle for instance whereas Maxwell's equations commonly are denoted in CGS-Gaussian units. Roussel-Dupré [6] is no different and uses CGS-Gaussian units for current densities and electric fields whereas the resulting formula for calculation of the conductivity is a mix. The CGS-Gaussian unit for electric potential or voltage is volt esu (electrostatic units) or statvolt implying that for instance electric field is measured in statV/cm. However, when presented with results one rarely finds these units. This inconsistent use of units is somewhat confusing and a word of caution is therefore in order to interpret the equations correctly. I have chosen to use CGS-Gaussian units for currents and conductivities as they relate more closely to the various formulae here presented. Electric fields on the other hand are presented in SI-units as this is more common both in American and European literature. The electric field units are related according to: 1 V/m = $1/3 \cdot 10^{-4}$ statV/cm.

3.2 Examples

To begin with it is of interest to compare λ_C as obtained by eq. (2.17) and that suggested by Roussel-Dupré, eq. (2.18). This is done in figure 3.1 from which it is evident that the two methods produce similar results. In the blue curve one can discern some influence from the layered structure of the U.S. Standard Atmosphere 1976 [9], used to calculate the air density, but overall the agreement is good. It may perhaps be argued that using eq. (2.17) is more "physical" in some sense but from a numerical viewpoint it seems clear that it can hardly matter which estimate is used. But to qualify this statement an examination of the γ-flux is in order. This is done in figures 3.2 and 3.3, of which the latter shows a blow-up near the point-of-explosion. Using an exponential dependence on altitude has the advantage of allowing the attenuation

integral in eq. (2.20) to be evaluated analytically. Figures 3.2 and 3.3 show calculations using numerical and analytic integrals as well as calculations using eq. (2.19). (As expected the numerical estimate of the z-dependent expression only confirms the analytic result and its only merit is to show that the numerical integration is reliable.) It is quite clear from these figures that near the point-of-explosion, the difference between the calculations are negligible and that they do not start to differ appreciably until they have dropped several orders of magnitude which they do within a few kilometers. It is therefore tempting to conclude that for the transverse components of the electric field it does not really matter which one is used and to some extent it may be true. The actual result, however, depends on current density and conductivity in a counteracting way. For small values of the integration variable the current density is large but then also large values of the conductivity are included in the exponent of the integrating factor. Further out the integrating factor will be close to 1 but then the current density is small. A closer examination of the behaviour of the integrands is therefore necessary. For the radial field, however, the situation is quite the opposite and integrating the γ-attenuation is critical as the results would otherwise be severely underestimated. Indeed, even the way in which λ_C is determined is critical if the observation point is far from the explosion as the difference between the z-dependent and the ρ-dependent γ-flux with integrated attenuation is several orders of magnitude at the far end in the diagram. Of course, the current densities and the conductivity also critically depend on the γ-attenuation estimate far away from the burst. To conclude this discussion it probably doesn't matter much whether eq. (2.17) or (2.18) is used for the transverse electrical fields but for the radial field it may be critical.

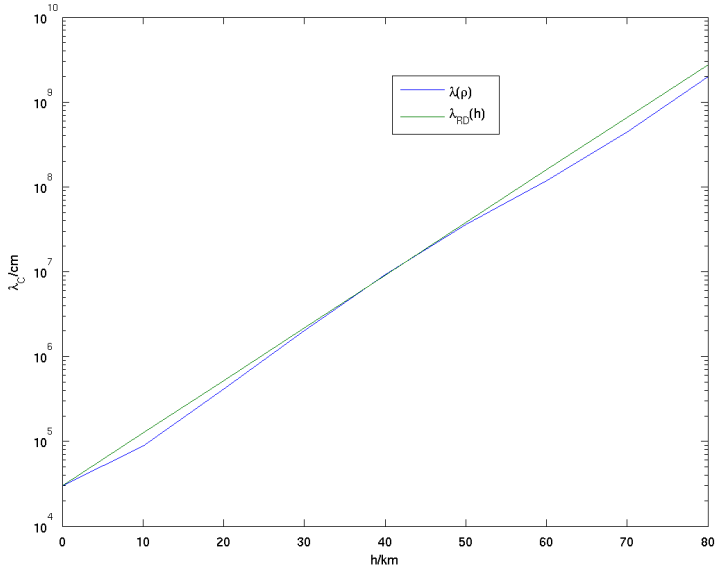

Figure 3.1: Comparison between λ_C as given by the present model's suggested estimate, blue curve, and that given by Roussel-Dupré, green curve. The legend indicates each estimate's primary dependence.

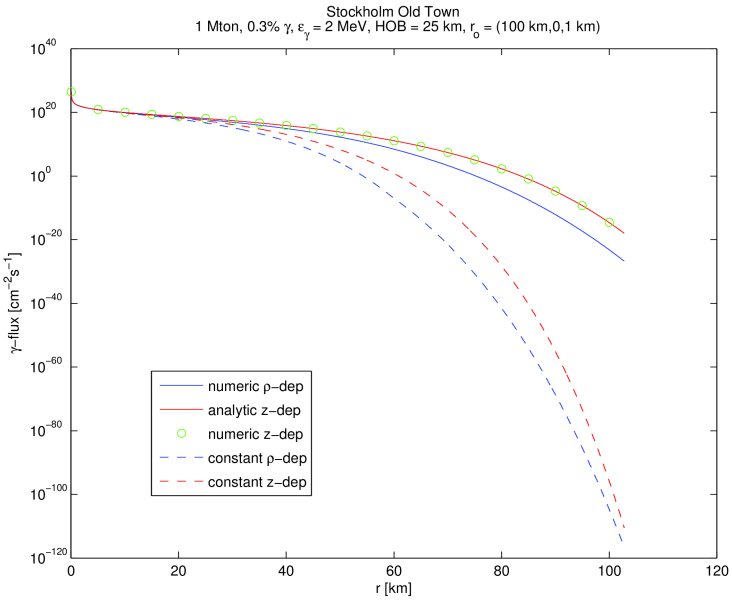

Figure 3.2: Comparison of the two expressions for the γ-flux. The top three labels correspond to eq. (2.20) and the bottom two to eq. (2.19). The term ρ-dep indicates that λ_C has been calculated according to eq. (2.17) and z-dep indicates eq. (2.18). The calculations are done for a 1 Mton burst over Stockholm and positions anywhere on the line connecting the point-of-explosion with a field point 100 km east of Stockholm at an altitude of 1 km as indicated above the figure.

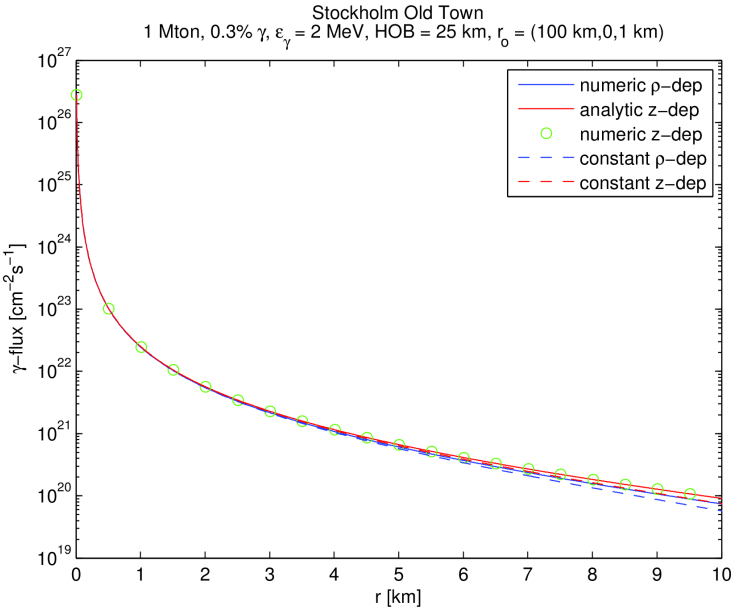

Figure 3.3: A magnification of the region closest to the point-of-explosion in figure 3.2.

3.3 Polar Components of the Current Density and Conductivity

The electric field components are all integrals over the corresponding current density components and an integrating factor containing the secondary electron conductivity. Therefore, some understanding of the electric field will be obtained by studying the current density components and the secondary electron conductivity. Figure 3.4 shows the current density components as obtained by the present model and Roussel-Dupré's. For the calculations the following parameters have been used:

- Compton electron energy: 1 MeV
- Longitude of nuclear explosion: 0°
- Latitude of nuclear explosion: 70° N
- Altitude of nuclear explosion: 25 km
- Nuclear yield: 1 Mton
- Mean γ energy: 2 MeV
- γ efficiency: 0.3 %

The field point is at an altitude of 1 km and directly above ground zero which is the point on the surface of the earth directly below the explosion. The magnetic field is obtained using a model published by IAGA, see ref. [17]. The model is essentially an expansion in spherical harmonics where the coefficients depend on time as the magnetic poles move around. The date set for the calculation of the magnetic field is 2005-01-01. The polar angle θ between the vertical line-of-sight and the geomagnetic field is in this case just under 12°. Note also that the calculations are not self-consistent with respect to the magnetic field and the current density.

Comparing Roussel-Dupré's model and the present in the figure the most obvious difference is that the former yields a larger magnitude of the radial component and smaller magnitudes of the transverse components. The difference stems from the fact that the present model treats the loss of Compton electrons at the same level of approximation as the equation of motion, eq. (2.1), for the Compton electrons whereas Roussel-Dupré utilises the simplification mentioned above in section 2.1. For the same reason, the results of the present model current densities are also a bit slower to rise as the Compton electrons suffer losses immediately. Comparison have been made between the current densities for each model using the analytic integral of the γ attenuation. The two models yield, however, results roughly of the same order of magnitude, i.e. the rather crude treatment of the Compton electron loss in Roussel-Dupré's model does not seem to have a dramatic influence on magnitude. That the behaviour is opposite for the transverse and radial components reflects conservation of charge as the same total number of electrons are generated for both models.

Another striking difference seen in the figure is that the amplitude of the radial current density is much larger than those of the transverse components. The reason for this is partly the rather small angle, θ, which means that the trigonometric part of the j_r integrand is considerably larger than those for the other components. Also the value of the trigonometric part for the r-component at $\tau = 0$ equals one whereas it is zero for the transverse components meaning that the j_r-integral starts to grow immediately whereas the transverse

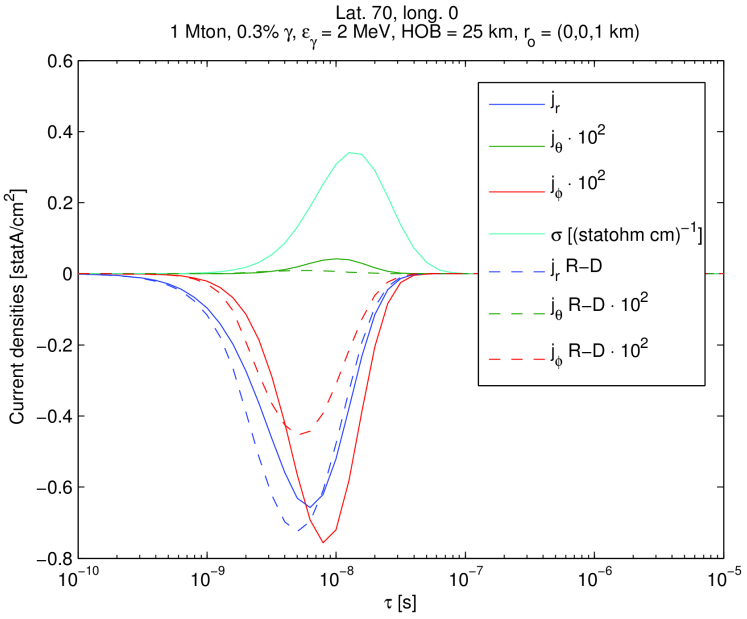

Figure 3.4: Polar components of the current density as given by the present model (solid lines) and Roussel-Dupré's (dashed lines). Note that in order to accommodate the components in one graph some of them are up-scaled with a factor indicated in the label box. The conductivity as given by eq. (2.28) and (2.29) is also shown sharing the numbers on the y-axis with the current density components.

components get no contribution until the trigonometric parts start to deviate from zero. This ties in well with the observation made above in the end of section 2.1. The trigonometric parts also undergo several oscillations during the retarded time interval but the oscillations are not seen because of exponential decrease in F_γ and electron loss. The θ-component is a bit slow compared to the other two which can be understood by examining the trigonometric parts of the respective integrands of the current components which for small time arguments are constant, quadratic and linear for the r-, θ- and ϕ-components respectively and accordingly a closer look reveals that the r-component comes first.

The conductivity rises later than the currents because its main contribution, in fact the only one in this estimate, is ionisation of air molecules by Compton electrons. Of course, there have to be some Compton electrons present before they can start to ionise, a process which takes some time.

Save for the reduction of the magnitude of the electric field, caused by the integration factor, the radial field is an integral over the retarded time of the current density. The shape of the radial current component therefore suggests that the radial electric field will rise from zero and saturate at some value. In fact, the saturation level of the radial component is given by the stationary solution of eq. (2.21). Calculations of the radial field for this field point presented further down verifies this, see figure 3.6.

As the transverse components of the electric field are integrals over r it is more informative to study the r-dependence of the current components and the secondary electron conductivity. Figure 3.5 below shows this dependence for the θ- and ϕ-components of the current density as well as the conductivity

for $\tau = 4 \cdot 10^{-9}$ s, which is close to the maximum amplitude of the current components. As the ϕ-component is negative only its magnitude has been considered in the logarithmic plot. The behaviour of the curves, not surprisingly, reflects that of the γ-flux using integrated attenuation shown in figure 3.2 and hence substantiating the contentions regarding consequences for the various electrical quantities made in that section. Comparing the present model and Roussel-Dupré's it is clear that closer to the detonation the transverse current components of Roussel-Dupré's model are larger meaning that corresponding transverse field components will be larger.

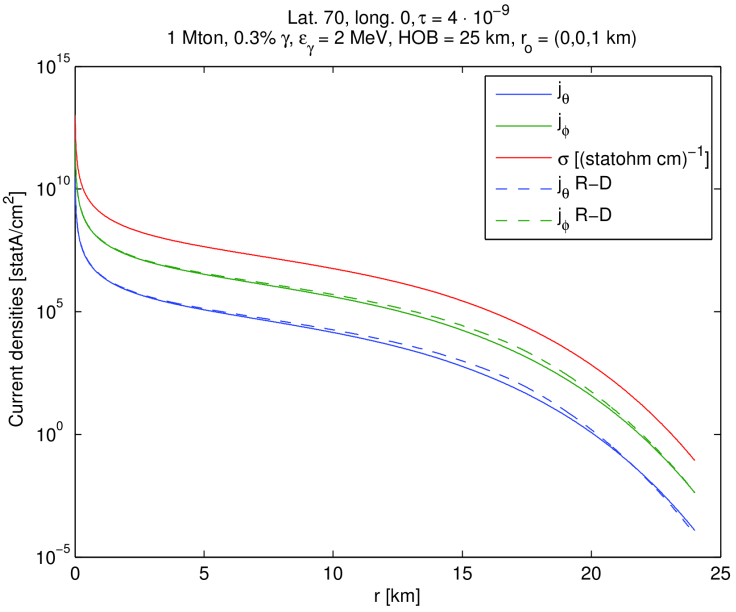

Figure 3.5: The dependence on distance from the explosion for the transverse current densities and the conductivity, the latter sharing the y-axis numbers with the current components. As the ϕ-component is negative only its magnitude is shown due to the logarithmic scale.

Taking into account that the figure exhibits monotonous dependence on r it is reasonable to expect that the transverse electric fields will exhibit a time dependence more or less similar to that of the γ-pulse, Fig. 2.2. Sufficiently far away from the nuclear burst this is true, see section 3.5.

3.4 Polar Components of the Electric Field

Figure 3.6 shows the magnitude of the electric field and all components as obtained by the present and Roussel-Dupré's model. All calculations have been done using the analytic integral for the γ attenuation. To accommodate all curves in the same graph some of the components are up-scaled. Clearly the electric field is dominated by the synchrotron contribution, E_ϕ. The r-component confirms the prediction regarding shape in the previous section. Again there is no dramatic difference between the present and Roussel-Dupré's model regarding the treatment of the Compton electron loss. The level of the r-component is much smaller than the transverse components, a fact that has been observed earlier, cf. ref [4]. Looking at the transverse components, however, there is quite a bit of difference between the two models. The most notable difference is that the features of the present model are smoother, no

doubt a result of the improved treatment of the Compton electron loss. The trailing hump of the total field (a second peak in Roussel-Dupré's model) is at present not quite accounted for and closer examination of current and conductivity is required. The field levels are not very large which is a bit surprising and also causes concern since the secondary electron mobility depends on the electric field. The sea level value used in eq.(2.30) corresponds to fields in the order of 10^4 V/m and clearly, there is a mismatch. In some situations, though, the model does give results in that order, see section 3.5. Another interesting observation is that the transverse fields peak well before the current components do which indicates that the decrease in amplitude due to the conductivity kicks in very soon. Again, this stresses the importance of accurately estimating λ_C.

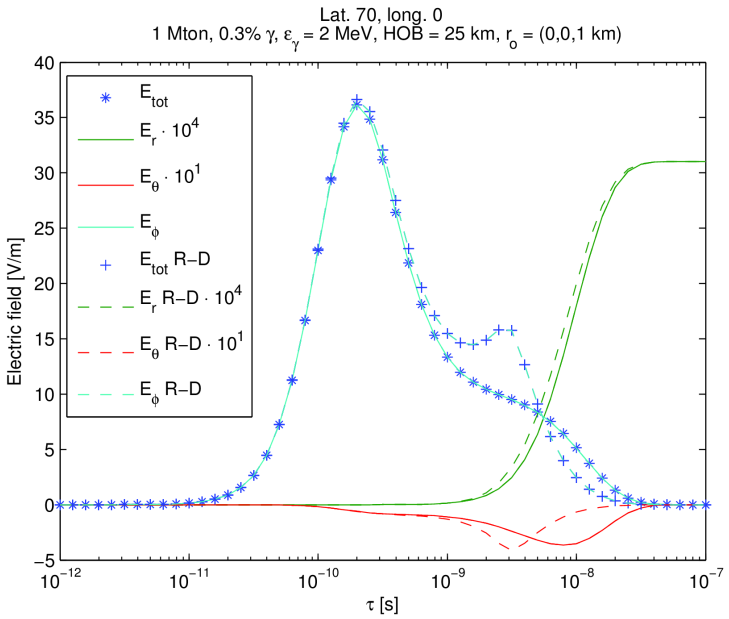

Figure 3.6: The total and polar components of the electric field for the present and Roussel-Dupré's model, the latter indicated by the letters R-D.

the

3.5 Comparison with other calculations

One is hard pressed to find results that make comparison worth while in the public EMP literature. Most figures are without numbers or units on the axes and if these are given then there is not enough information regarding parameters to enable corresponding calculations. So far, the search has only resulted in one usable figure found on a blog on the Internet [18]. The original is shown below, figure 3.7.

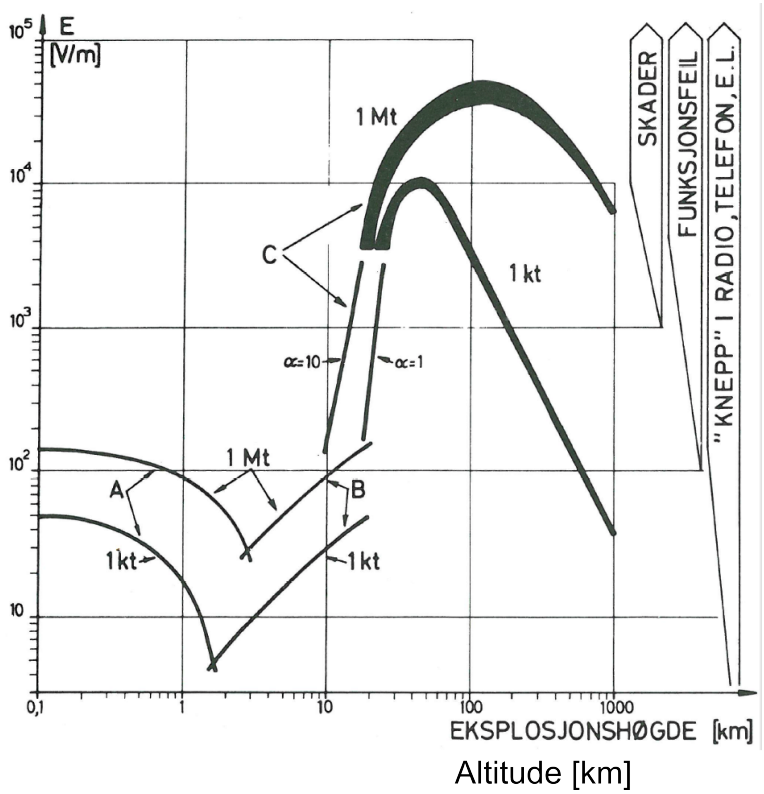

Figure 3.7: Maximum EMP at a distance of 100 km from ground zero. The letters A,B and C denote different EMP generating mechanisms: A air-ground discontinuity, B air density gradient and C magnetic interaction. Reproduced by express permission from Karl-Ludvig Grønhaug. (Translations, see footnote.)

The figure[1] originates from a Norwegian EMP handbook [19, Fig. 4.1] produced in the late seventies. From this figure one can see that a one Mton bomb will give a peak amplitude of just under 10 kV/m for an explosion altitude of 25 km. Figure 3.8 shows the result of the present model for a burst over Stockholm Old Town (lat 59.3°, long 18.3°) at an altitude of 25 km. The field point is 100 km east of ground zero, at an altitude of 1 km and the date is set to 2012-01-01. Other parameters are the same as in the previous case. Clearly, the present model gives a peak of a much smaller magnitude than the one indicated in figure 3.7. One can also see that the saturation level of the radial field is much smaller compared to the transverse fields than was the case in figure reffig:lat70-z1-fields. At this distance the dominance of the synchrotron contribution E_ϕ, eq. (2.25) is even more pronounced.

[1] Fig. 3.7 glossary: skader=damage, funksjonsfeil=malfunction, "knepp" i radio, telefon,

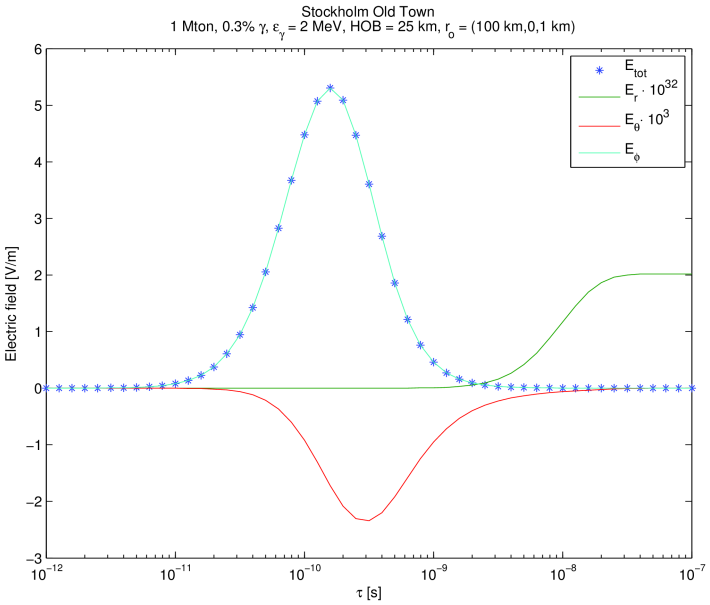

Figure 3.8: Electric field components and the total a 100 km east of Stockholm at an altitude of 1 km as obtained by the present model, ($\theta = 75.6°$). Note that some components have been up-scaled.

Figures 3.9 - 3.13 show the field at an altitude of 10 km for some lateral distances from ground zero along the meridian. The altitude is interesting as commercial aircraft commonly fly at this altitude but also because one can be certain that there will be no contribution from the ground.

Note that the radial field in figures 3.9 - 3.13 has a peak that is comparable to and mostly also larger than the synchrotron contribution. Note also that at this altitude the magnitude of the electric field is several orders of magnitude larger than at 1 km altitude, see figure 3.6. The radial and synchrotron peaks also vary over the range of positions but in different fashions. The synchrotron contribution has a minimum somewhere near 5 km north of ground zero and is larger on the south side than on the north whereas the r-component is more or less symmetric around ground zero. The variation of the synchrotron contribution is a result of the different angles, θ in figure 2.1, between the line-of-sight and the direction of the magnetic field of which the latter has an inclination of about -73°. At 5 km north of ground zero θ is very small, only about 2°, making the primary electrons go almost parallel to the magnetic field yielding a very small magnetic force. As θ grows on either side of 5 km north the synchrotron contribution also grows until eventually the increase is overpowered by the $1/r$-dependence in eq. (2.25). Therefore there is a peak value at some lateral distance from the minimum point.

The peak in the radial field is not so easy to understand but is a result of the interplay between radial current and conductivity. More information is needed to give a clear explanation. Similar curves have been given for the radial field resulting from a burst much closer to the ground [20, Fig.15] and [21, Fig.6-9]. In this case there is a contribution from the ground reflex but this is relatively small. Some more properties of the radial field will be demonstrated further

e.l.= klick and pop noise in radio, telephone etc.

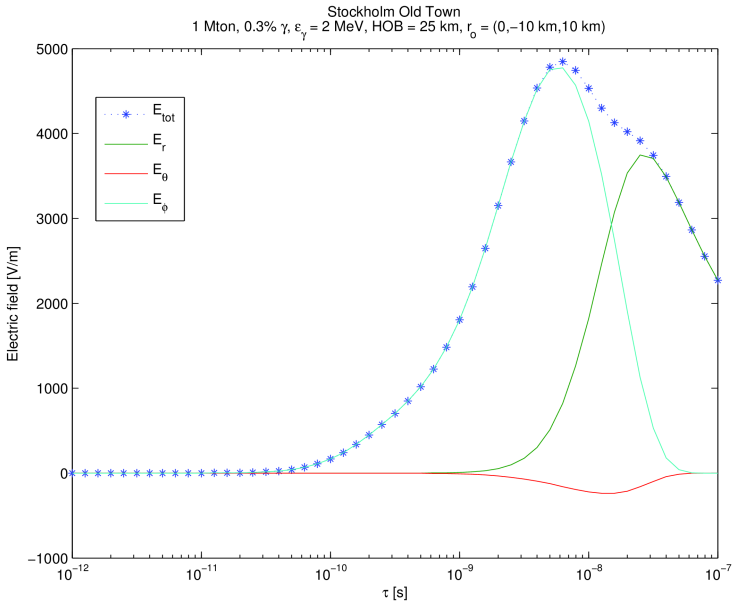

Figure 3.9: Total electric field and polar components 10 km south of ground zero at an altitude of 10 km, (θ=51.0°).

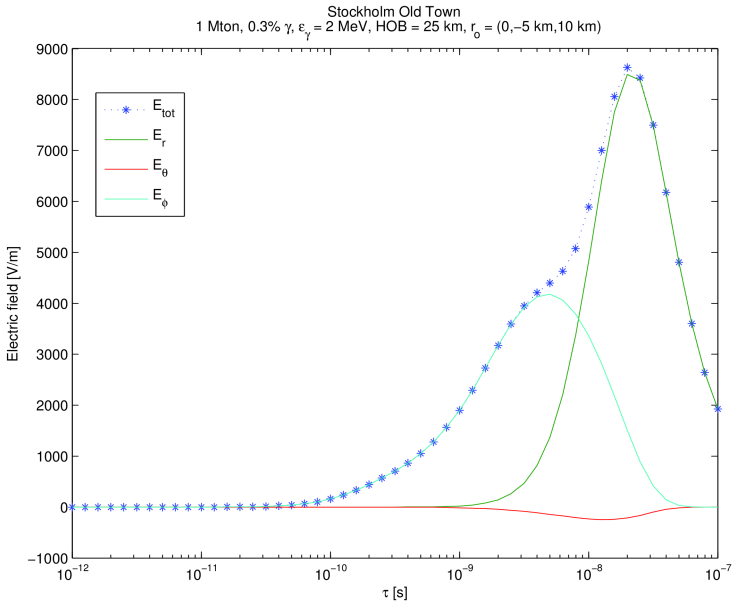

Figure 3.10: Total electric field and polar components 5 km south of ground zero at an altitude of 10 km, (θ=36.0°).

down.

Figure 3.14 shows the maximum of the electric field, E^{max}, and the maximum radial field, E_r^{max}, along the meridian through Stockholm Old Town, still at an altitude of 10 km for the present and Roussel-Dupré's model. Figure 3.15 shows similar curves but this time along the latitude. There is a notable dominance around ground zero of the radial field and this extends to roughly

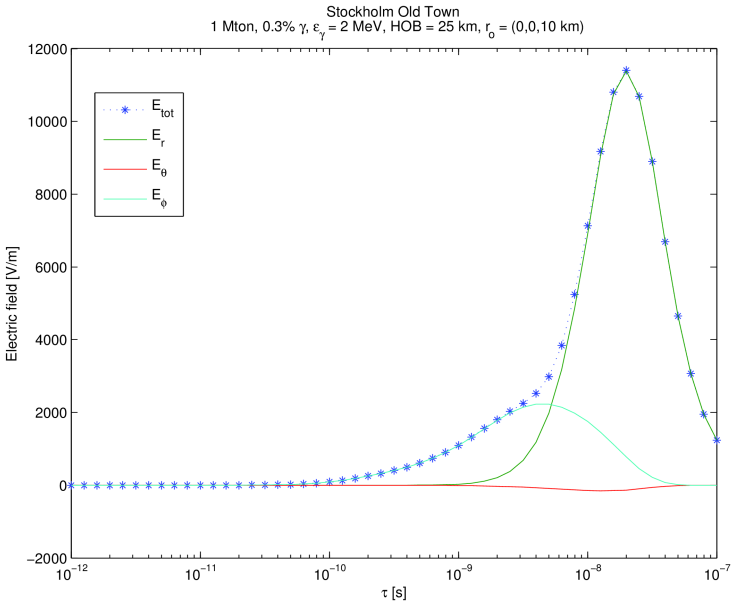

Figure 3.11: Total electric field and polar components above ground zero at an altitude of 10 km, (θ=17.4°).

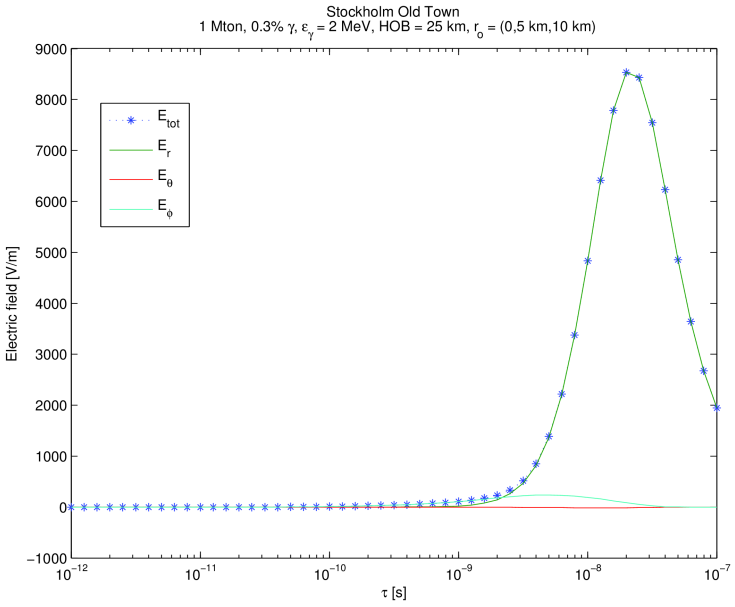

Figure 3.12: Total electric field and polar components 5 km north of ground zero at an altitude of 10 km, (θ=1.9°).

half the explosion altitude. Further out, though, the synchrotron contribution dominates. The clear asymmetry in fig. 3.14 is caused by the change in θ. One can also see that Roussel-Dupré's model at this altitude gives larger total field as figure 3.5 indicates. Somewhat surprisingly also the r-component is larger but that may be an effect of the conductivity. It would have been interesting to see also the value of the saturation level but the program used for calcula-

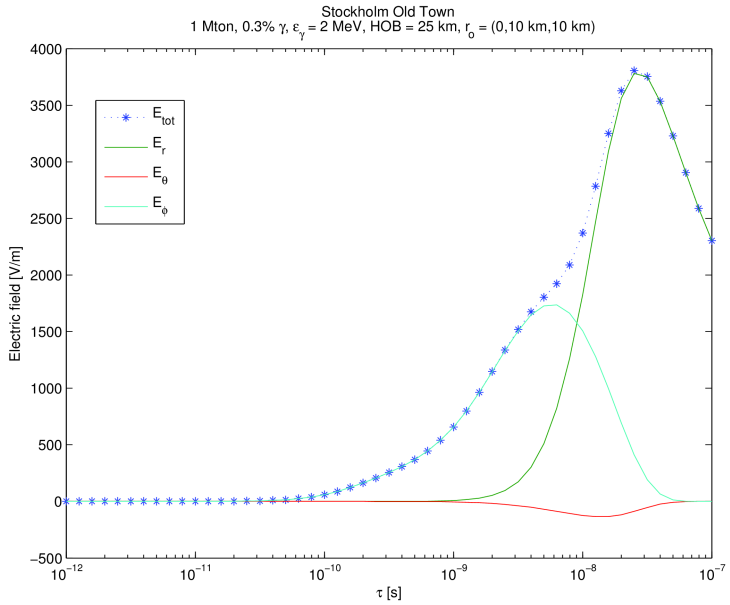

Figure 3.13: Total electric field and polar components 10 km north of ground zero at an altitude of 10 km, (θ=16.4°).

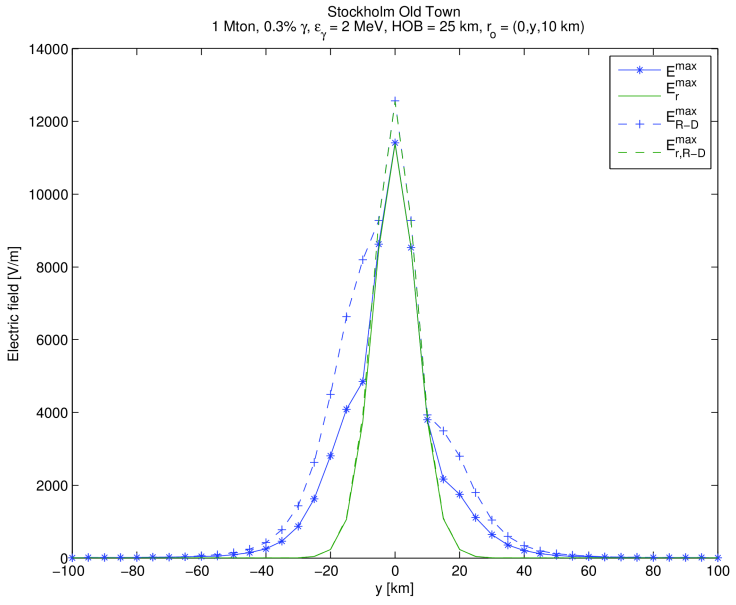

Figure 3.14: Peak of electric field and maximum radial field along the meridian through Stockholm Old Town at an altitude of 10 km.

tions times out during the integration for the larger τ-values for reasons as yet unknown.

Figures 3.16 and 3.17 show corresponding curves but at an altitude of 1 km, this time without Roussel-Dupré's model. In this case the results are almost equivalent and adding the curves would only clutter the view. The radial field has been up-scaled a factor of 10^4 in order to show within the figure. The

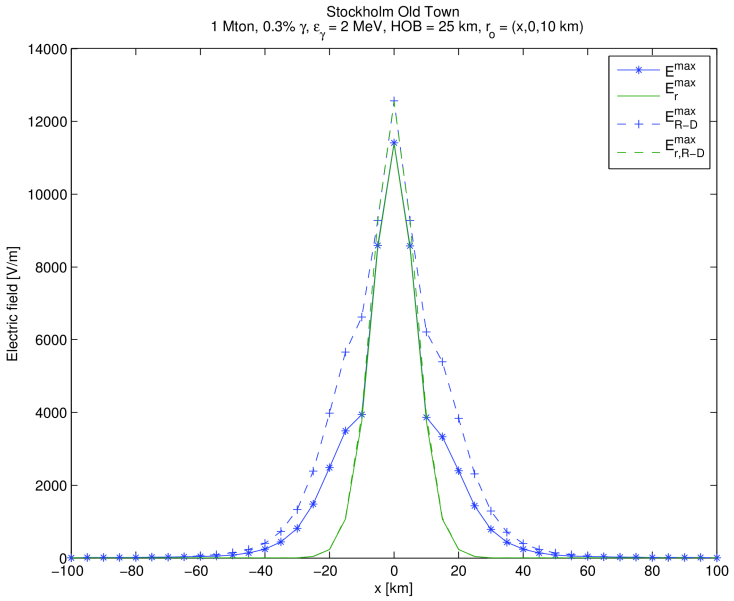

Figure 3.15: Peak of electric field and maximum radial field along the latitude through Stockholm Old Town at an altitude of 10 km.

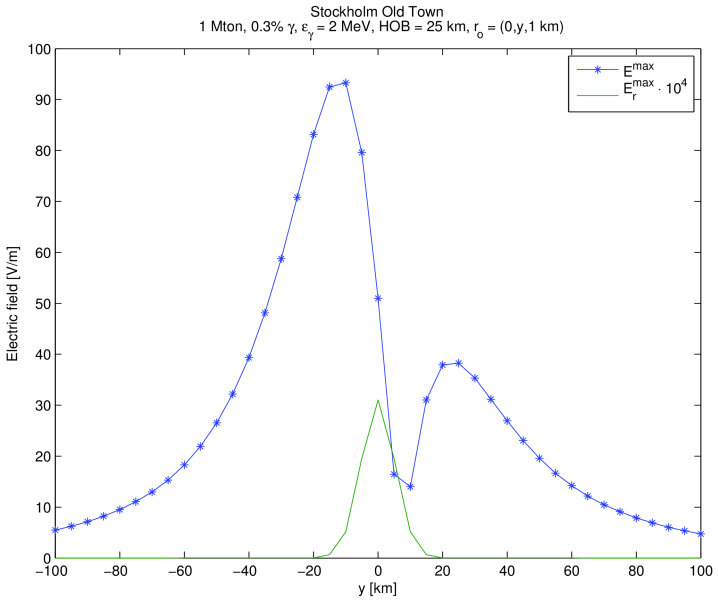

Figure 3.16: Peak of electric field and maximum radial field along the meridian through Stockholm Old Town at an altitude of 1 km. The radial field has been up-scaled a factor of 10^4.

shape of E^{max} in these figures is entirely consistent with EMP contour plots published on the Internet [13] and elsewhere, e.g., ref. [22, 23, 24] showing a "happy face" symmetric about the magnetic north. In Stockholm the magnetic north is east of the geographic north and hence E^{max} is not symmetric around the origin in figure 3.17. Also here the minimum is caused by minimum θ

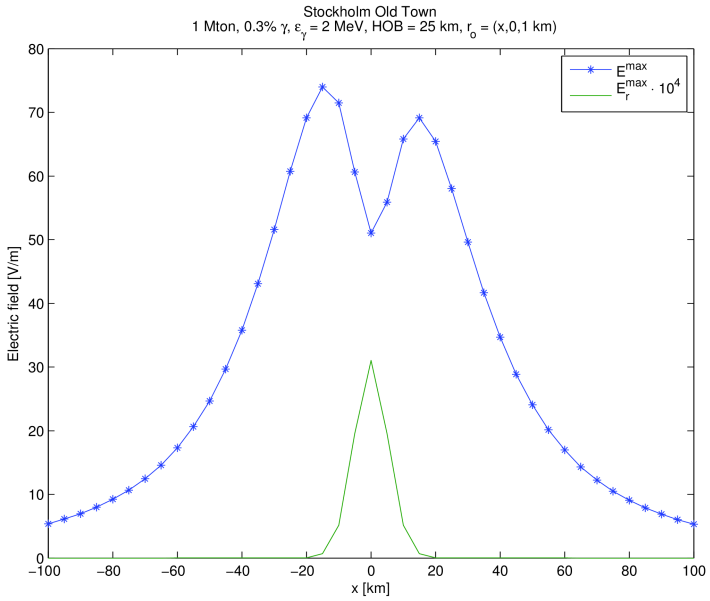

Figure 3.17: Peak of electric field and maximum radial field along the latitude through Stockholm Old Town at an altitude of 1 km. The radial field has been up-scaled a factor of 10^4.

but occurs at "ground zero". E_r^{max} on the other hand is symmetric around the origin in both figures. In fact, circular symmetry in the lateral plane is suggested for the radial component. Note also that the drop in radial field as the lateral distance increases is much larger than that for the transverse fields. This is true also at 10 km altitude.

The peak in the radial field coming shortly after the synchrotron peak is not present at an altitude of 1 km above ground zero as is evident by figures 3.6 and 3.8. In fact, calculations have shown that it is not present already at an altitude of 5 km. Clearly the features of the radial field depend on distance from the burst in a way not easily explained by γ attenuation and spherical spread alone and further studies are required to understand the radial field behaviour, as has been pointed out above. Taking away the magnetic force from the current differential equation (2.3) decouples the Cartesian coordinates associated with the polar coordinate system and enables straight forward integration. A study of this solution will verify if the radial field features at all have something to do with the magnetic interaction in some way or not. The evidence so far suggests that the radial field is not affected by the magnetic interaction beyond the loss due to primary electrons being deflected from the line-of-sight.

4 Discussion and Outstanding Issues

A substantial understanding of the theory presented above and relative importance of parameters has been gained from the example calculations and many features can be understood from basic physics. However, the calculated levels are not in accord with independent results. The examples have also revealed some effects not entirely understood, namely the peak in the radial field and the behaviour of the synchrotron contribution relatively close to the burst. A potentially serious shortcoming is that the calculations are not self-consistent in currents and magnetic field. However, other results available from various sources generally also suffer from this. An exception is [25, Fig. 6 and 7] which maintains that self-consistency, not surprisingly, adds to computational time. The presented figures indicate that self-consistency yields somewhat lower but otherwise similar results. However, some observations hold also for the case of self-consistent calculations. The upper limit on the magnitude of the electric field obtained when dropping the integration factors is an example. It is also very likely that only the first few kilometres from the burst will have an appreciable influence also for self-consistent calculations of transverse fields. It will probably not have a big influence whether the present model or that of Roussel-Dupré is used except in the vicinity of the burst. In fact most of the observations of qualitative properties stated above will probably hold. Moreover, regardless of where the field point is relative to the point of explosion the C++ program always uses the same value for the magnetic field. This may have negligible influence if one considers field points which have the same latitude as the point of explosion. The geomagnetic variation along a latitude is moderate but along a meridian the geomagnetic field changes more rapidly and even comparatively short distances may have severe influence in particular if the direction of the magnetic field changes. It may, however, be that over the region in which the flat earth approach is reasonable, the magnetic field does not vary appreciably and if so the use of a constant magnetic field is justified. The relatively small region around the nuclear burst contributing to the transverse field also strengthens the case for a constant magnetic field. A problem with using a local magnetic field is that the definition of the polar coordinates will change if the direction of the magnetic field changes. Only the radial coordinate is invariant which means that the transverse components of the field cannot be distinguished from one another. Hence only the radial component can be determined separately but maybe it suffices. It is possible to overcome this obstacle if all subsequent calculations of current components in the field integrals are converted to a coordinate system independent of the magnetic field direction. Other caveats regarding the results are that not very many field points have been investigated and also that not much effort has been made regarding the parameters that have influence on the population of secondary electrons.

4.1 Conclusions

Observations made during the course of this work have resulted in the following conclusions:

- Many features found during the calculations are completely understood and can be related to basic physics.
- The numerical results of the present and Roussel-Dupré's model are not

very different, i.e. the crude treatment of the loss of primary electrons in Roussel-Dupré's model seems not to have any serious consequence except relatively close to the nuclear explosion.

- The exponential, or near exponential, dependence on altitude of several parameters must be taken into account if currents or conductivity are/is of interest. Also the radial field at large distances critically depends on an accurate estimate of the γ mean free path.
- Transverse currents far from the nuclear burst do not contribute significantly to the EMP suggesting that constant values of some parameters will give reasonable estimates of transverse fields.
- The properties of in particular the radial field but also some features present in the transverse components are not entirely understood.
- The level of the radial field at altitudes of 10 km and above gives reason for concern regarding commercial aircraft.
- The numerical results presented here are not always consistent with independent results and in some situations results are not consistent with assumed values of some parameters.

4.2 Way ahead

The various shortcomings mentioned above may be transformed into a shortlist of things to address in future work, not necessarily in order of priority.

- An extensive parameter study is recommended to investigate further the properties of the radial field. In order to facilitate this the speed of the computer program must be increased. The calculation of the electric field components requires several nested integrations which consume a lot of time. This is the reason for the rather sparse field points calculated so far. Using instead Monte Carlo techniques for the integration should increase the speed of the field calculations. The failure of the integration for large τ-values must also be remedied.
- The sometimes rather large discrepancies between the present results and earlier public ones must be investigated. A first step could be to look into properties of the γ mean free path.
- To facilitate comparison with in-house independent calculations, the set of input parameters must be decided on and also the user interface which includes modification to allow for field point specification using latitude and longitude, i.e. no more flat earth.
- Investigation of model properties without magnetic interaction will tell if there is indeed some coupling to the radial field with the magnetic interaction. Of course one needs to take into account that all electrons rather than just some in this case contribute. The calculations have shown, though, that it is a relatively small amount of electrons that do deviate from the radial direction, at least directly below the nuclear blast and it may prove sufficient to consider only points directly below the blast as in this case the mysterious features are most prominent.
- An investigation of the potentially serious limitation of not doing self-consistent calculation of currents and magnetic field must be done. A

first Born approximation is suggested to begin with. Likewise the effect of using constant magnetic field must be assessed. This may be addressed by simply changing the code to allow for local magnetic fields and see if there is a significant difference. In doing so the introduced uncertainties regarding the polar angle coordinates must be borne in mind.

- Extension of the theory and program to high altitude explosions. Here the secondary electrons must be treated differently as the atmosphere is much thinner.
- Investigation of the reactions of the secondary electrons with the air molecules is still on the list [15].

Of maybe lesser importance is:

- Modification of some parameter estimates to better allow for the dependence on altitude.
- Investigation of other asymmetry generators, e.g., weapon design or air-ground interface.
- Generate graphs in real time during calculation perhaps by integration of the program with MATLAB.
- A GUI front end where parameters may be set.

4.3 Acknowledgements

This work has benefited from IAGA [17] which provides an executable to calculate the magnetic field. PDAS [9] must be mentioned in connection with the calculation of atmospheric properties. Thanks also go to Robert Roussel-Dupré, the author of [6], for fruitful e-mail correspondence. Many valuable suggestions have also been done by colleagues.

Bibliography

[1] W.J. Karzas and R. Latter. The Electromagnetic Signal Due to the Interaction of Nuclear Explosions with the Earth's Magnetic Field. *J.Geophysical Research* ***67****(12),4635*, 1962.

[2] W.J. Karzas and R. Latter. Electromagnetic Radiation from a Nuclear Explosion in Space. *Phys.Rev.* ***126****(6),1919*, 1962.

[3] W.J. Karzas and R. Latter. Detection of the Electromagnetic Radiationfrom Nuclear Explosions in Space. *Phys.Rev.****137****,B1369*, 1965.

[4] C.L. Longmire. On the Electromagnetic Pulse Produced by Nuclear Explosions. *IEEE Trans. Antennas and Propagation,* ***AP-26****(1),3-13*, 1978.

[5] C.E. Baum. From the Electromagnetic Pulse to high-power electromagnetics. *Proc. IEEE ,* ***80****(6),789-817*, 1992.

[6] R.A. Roussel-Dupré. Prompt Nuclear EMP and Synchrotron Radiation: A Resolution of Two Approaches. *IEEE Trans. Electromagnetic Compatibility* ***47****(3),552-558*, 2005.

[7] R.A. Roussel-Dupré. Private communication.

[8] Bo Thidé. *Electromagnetic Field Theory.* Plasma Theory Group, Uppsala university, 2010-03-08. Online draft, `http://www.plasma.uu.se/CED/Book/`.

[9] `http://www.pdas.com/atmos.html`.

[10] `http://en.wikipedia.org/wiki/International_Standard_Atmosphere`.

[11] L.W. Seiler. A Calculational Model for High Altitude EMP. *NTIS AD-A009 208*, 1975.

[12] C.L. Longmire. Justification and Verification of High-altitude EMP Theory. C.E. Baum, Theoretical notes, `http://www.ece.unm.edu/summa/notes/Theoretical.html`, 1986.

[13] `http://en.wikipedia.org/wiki/High-altitude_nuclear_explosion`.

[14] J.S. Malik. The Compton Current. C.E. Baum, Theoretical notes, `http://www.ece.unm.edu/summa/notes/Theoretical.html`, 1965.

[15] G. Ljungdahl. Nuclear Explosion generated EMP: Field Calculations. *FOI-R–2489–SE*, 2008.

[16] Carl Nordling and Jonny Österman. *Physics Handbook.* Studentlitteratur, 1980. ISBN 3-88598-007-X.

[17] `http://www.ngdc.noaa.gov/IAGA/` and `http://www.ngdc.noaa.gov/geomag/models.shtml`.

[18] `http://glasstone.blogspot.se/2006/03/emp-radiation-from-nuclear-space.html`.

[19] Karl-Ludvig Grønhaug. Elektromagnetisk puls håndbok 1978. *Intern rapport F-657 Forsvarets forskningsinstitutt, Norway*, 1978.

[20] J.R. Legro, N.C. Abi-Samra, A.R. Hileman, and F.M. Tesche. Study to Assess the Effects of Nuclear Surface Burst Electromagnetic Pulse on Electric Power Systems. *Oak Ridge National Laboratory, Sub/83-44374/1/V4*, 1985.

[21] C.L. Longmire. Theory of EMP Coupling in the Source Region. C.E. Baum, Theoretical notes, `http://www.ece.unm.edu/summa/notes/Theoretical.html`, 1980.

[22] Ed. P.J. Dolan. Capabilities of Nuclear Weapons, part 1. DNA EM-1, `http://www.alternatewars.com/WW3/WW3_Documents/WW3_Documents.htm`, 1972.

[23] S. Glasstone and P.J. Dolan. The effects of nuclear weapons. `http://www.alternatewars.com/WW3/WW3_Documents/WW3_Documents.htm`, 1977.

[24] K.D. Leuthäuser. A Comlete EMP Environment Generated by High-Altitude Nuclear Bursts: Data and Standardization. C.E. Baum, Theoretical notes, `http://www.ece.unm.edu/summa/notes/Theoretical.html`, 1994.

[25] K.D. Leuthäuser. A Comlete EMP Environment Generated by High-Altitude Nuclear Bursts. C.E. Baum, Theoretical notes, `http://www.ece.unm.edu/summa/notes/Theoretical.html`, 1992.

FOI, Swedish Defence Research Agency, is a mainly assignment-funded agency under the Ministry of Defence. The core activities are research, method and technology development, as well as studies conducted in the interests of Swedish defence and the safety and security of society. The organisation employs approximately 1000 personnel of whom about 800 are scientists. This makes FOI Sweden's largest research institute. FOI gives its customers access to leading-edge expertise in a large number of fields such as security policy studies, defence and security related analyses, the assessment of various types of threat, systems for control and management of crises, protection against and management of hazardous substances, IT security and the potential offered by new sensors.

FOI
Defence Research Agency
SE-164 90 Stockholm

Phone: +46 8 555 030 00
Fax: +46 8 555 031 00

www.foi.se